ISBN: 978-3-95450-223-3 ISSN: 2673-7000 doi:10.18429/JACoW-NAPAC2019-WEYBB1

ELENA COMMISSIONING*

D. Gamba†, M.E. Angoletta, P. Belochitskii, L. Bojtar, F. Butin, C. Carli, B. Dupuy, Y. Dutheil, T. Eriksson, P. Freyermuth, C. Grech[1], M. Hori[2], J.R. Hunt, M. Jaussi, L. V. Joergensen, B. Lefort, S. Pasinelli, L. Ponce, G.A. Tranquille, CERN, Espl. des Particules 1, 1211 Meyrin, Switzerland
R. Gebel, Jülich Institute for Nuclear Physics, Jülich 52425, Germany,
[1]also at University of Malta, MSD 2080 Msida, Malta,
[2]also at Max Planck Institute Quantenopt., Munich D-80799 Germany

Abstract

The Extra Low ENergy Antiproton storage ring (ELENA) is an upgrade project at the CERN AD (Antiproton Decelerator). ELENA will further decelerate the 5.3 MeV antiprotons coming from the AD down to 100 keV. ELENA features electron cooling for emittance control during deceleration thus preserving the beam intensity and allowing to extract bright bunches towards the experiments. The lower energy will allow for increasing the antiproton trapping efficiency up to two orders of magnitude, which is typically less than 1% with the present beam from AD. The ring was completed with the installation of the electron cooler at the beginning of 2018. Decelerated beams with characteristics close to the design values were obtained before the start of CERN Long Shutdown 2 (LS2). During LS2 electrostatic transfer lines from the ELENA ring to the experimental zones will be installed, replacing the magnetic transfer lines from the AD ring. The latest results of commissioning with H^- and antiprotons and the first observation of electron cooling in ELENA will be presented, together with an overview of the project and status and plans for LS2 and beyond.

INTRODUCTION

The Antimatter Experiments hosted at CERN [1] presently take antiproton beams from the AD [2]. The AD provides about 3×10^7 antiprotons per pulse with 5.3 MeV kinetic energy to experiments typically capturing them in traps. The experiments have to further decelerate the beam to an energy of a few keV to be able to trap them. This further deceleration is typically obtained by sending the beam through several thin foils (one experiment uses a RadioFrequency Quadrupole Decelerator (RFQD) [3, 4]). During the process most of the beam is lost, and the final trapping efficiency is of the order of 0.5%. Instead, ELENA [5] allows for controlled deceleration of the antiproton beam down to 100 keV with high transmission efficiency (nominal 60%) and keeping low transverse and longitudinal emittances thanks to the use of the electron cooling technique. It is expected that this will allow for increasing the experiments trapping efficiency by up to two orders of magnitude. ELENA has also the flexibility to produce up to four bunches of equal intensity and emittances which can be used to serve several experiments at the same time.

The ELENA project was approved at CERN in June 2011 and construction began two years later [6]. The first circulating H^- beam was observed in November 2016 [7], even though the ring installation was completed at the beginning of 2018 with the final installation of the electron cooler. The results presented in this proceedings have mainly been obtained in 2018, before the start of LS2.

ELENA OVERVIEW

Details of the ELENA design can be found in [5]. The ELENA ring has an hexagonal shape and its circumference is about 30 m. Figure 1 shows a picture of the ELENA ring after its complete installation, with the main components highlighted. Two slightly longer straight sections host the injection and the electron cooling. The other four straight sections host two fast deflectors [8] to extract the beam toward the experimental areas, one wide-band RF cavity and one wide-band longitudinal diagnostics, among three families of quadrupoles for optics control. The three quadrupole families allow for the adjustment over a certain range of the transverse tunes to avoid resonances and of the dispersion at the electron cooler in order to optimise the cooling process. Additionally, two families of skew quadrupoles and two families of sextupoles are installed for coupling and chromaticity correction, as well as two solenoids to compensate for the effect of the main solenoid of the electron cooler.

The 5.3 MeV pbar beam from AD is injected into ELENA from a 20 m long magnetic transfer line. Due to the low

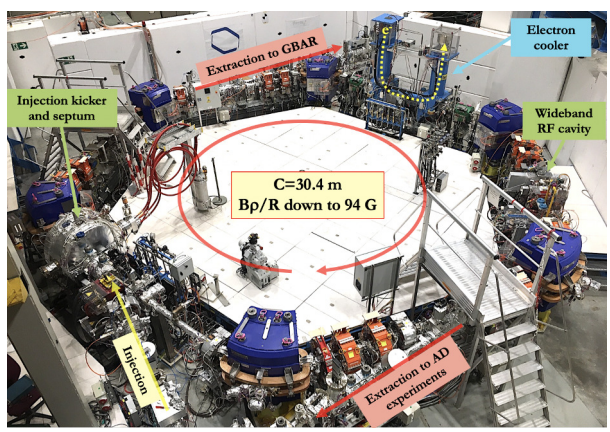

Figure 1: Picture of the ELENA Ring after installation. The main components are highlighted.

* Work supported by the ELENA Project
† davide.gamba@cern.ch

ISBN: 978-3-95450-223-3 ISSN: 2673-7000 doi:10.18429/JACoW-NAPAC2019-WEYBB1

extraction energy (100 keV), electrostatic transfer lines [9] were chosen to deliver beams to the experiments.

An ion source able to provide 100 keV H^- or proton beams is installed next to the injection/extraction transfer lines. It was conceived to provide beams for commissioning purposes, i.e. to gain in beam-time availability with respect to the slow (≈ 100 s) AD cycle, and eventually proceed with ELENA commissioning and/or optimisation in parallel to AD beam time dedicated to the antiproton physics program.

BEAM INSTRUMENTATION

Several beam diagnostic systems were installed and commissioned in ELENA [10].

Ten Beam Position Monitors (BPMs) allow for observing the horizontal and vertical beam position of the circulating bunched beam [11–13]. Two additional BPMs per plane are embedded in the electron cooler to help optimise the ion and electron beams overlap. The bunched beam position can be acquired already treated by dedicated Digital Down Converters (DDC) or as raw signal via Oasis, a virtual oscilloscope system [14].

A wide-band, low-noise, magnetic longitudinal pick-up (LPU) is installed. It was intended to provide inputs to the Low Level RF (LLRF) [15] beam phase loop as well as to be used for Schottky diagnostics to estimate the beam intensity and the energy spread of the coasting beam, thus allowing the optimisation of the cooling process. Despite a careful design and characterisation [13, 16] its expected performance has not yet been reached after installation. Attempts to improve it are under way. The BPMs were designed to have the possibility of merging all their sum signals to be used as distributed longitudinal Schottky pickup [5, 11]. However, a single BPM sum signal has enough Signal-to-Noise Ratio (SNR) and bandwidth and was used instead of the LPU for most uses.

Beam size measurements in the ring are possible via a scraper system [5, 10]. The scraper was designed to be able to measure both pbars and H^- or protons by measuring pions created by the pbar annihilation or secondary electrons generated by the ions interaction with the blade. Due to non-zero dispersion at the location of the scraper, a dedicated algorithm was developed [17] and used [18] for inferring the beam emittance. Such a measurement is destructive and systematic measurements of emittance evolution along the cycle are time consuming.

Two identical devices with four electrodes [10] are used to excite the beam and monitor coherent transverse oscillations via a dedicated processing electronics [19] which allows for measuring the beam tunes.

One Beam Current Transformers (BCT), similar to the LPU installed in the ring, is installed in each extraction line to measure the extracted beam intensity, while several non-destructive microwire monitors [20] are installed to provide the transverse beam profile and mean position. Figure 2 shows a typical beam profile measured in the extraction line toward the GBAR experiment. Unfortunately, the head

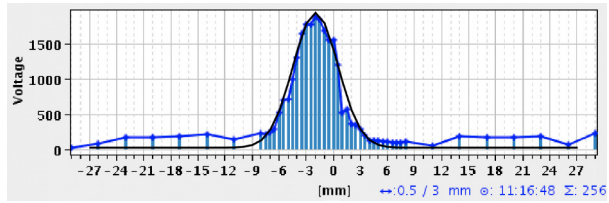

Figure 2: Ejected beam vertical profile measured by a microwire monitor.

electronics and acquisition system were still at prototype stage, therefore those profile monitors were only partially available for a limited amount of time toward the end of the run. Scintillation screens installed just after injection [10] were the only working solution to measure and optimise the incoming pbar and H^- beams, while a MicroChannel Plate (MCP) detector installed in the GBAR experiment was used as main beam diagnostics to set-up and optimise the corresponding extraction line.

H^- CYCLE

The ion source was characterised before connecting it to ELENA [21]. After its connection, the the H- beam was quickly brought to the ring as already reported in [7]. Due to breakdowns in the insulation transformer of the ion source the actual energy of the beam had to be reduced to 85 keV. Despite of the lower energy, it was possible to transport the beam to ELENA and quickly accelerate it to 100 keV or even to the nominal pbar injection energy of 5.3 MeV and decelerated back to 100 keV as shown in Fig. 3. The measured H^- lifetime was of the order of a few seconds, which is reasonably close to expectations given the measured vacuum pressure (a few 10^{-11} mbar). H^- beams were also used to debug and commission several equipment systems, in particular the LLRF [22], as well as for the first commissioning of the extraction line to GBAR [23].

Large shot-to-shot intensity fluctuation of the H^- beam were observed. This could be due to poor intensity stability along the H^- pulse produced by the ion source. Random shot-to-shot intensity fluctuations along the pulse were observed

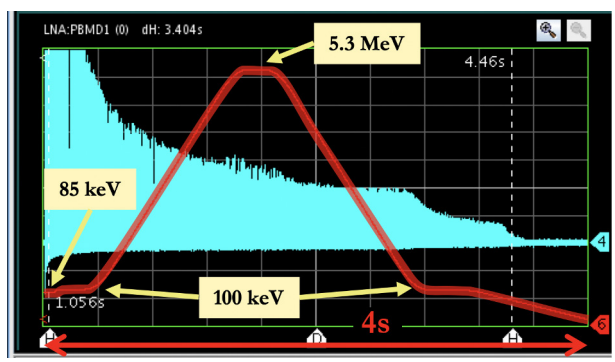

Figure 3: Typical accelerating cycle with H^-. The magnetic cycle is highlighted in red. The peak of the longitudinal beam line density from a BPM is in blue.

ISBN: 978-3-95450-223-3 ISSN: 2673-7000 doi:10.18429/JACoW-NAPAC2019-WEYBB1

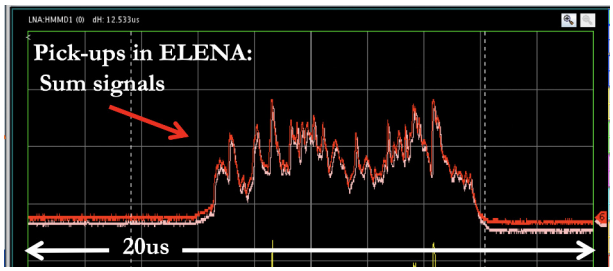

Figure 4: Sum signal of two consecutive BPMs in the ELENA ring just after injection of a 10 μs-long H^- beam.

by looking at the longitudinal beam distribution seen on the sum signal of two consecutive BPM just after injection, see Fig. 4. Note that only a 0.5 μs-long part of the 10 μs-long source pulse is normally injected in the ring, as this corresponds to the flat-top of the injection kicker.

Eventually, the ion source insulation transformer failed completely, preventing further use of ion beams. Despite several attempt to solve the problem with the insulation transformer, most of the ELENA commissioning had to be performed with limited pbar beam-time dedicated by AD to ELENA.

PBAR DECELERATING CYCLE

The typical pbar decelerating cycle is depicted in Fig. 5. Beam is injected as a single bunch from the AD at 100 MeV/c in a waiting RF bucket. A first deceleration step brings the beam to 35 MeV/c where the beam is debunched and the electron cooler is used to reduce the beam emittances. After being re-bunched, the beam is brought to 13.7 MeV/c where it is again debunched and cooled. The beam is finally re-bunched and extracted toward the experiments. By design, the final re-bunching is performed at harmonic four and the electron cooler is kept ON for "bunched beam cooling" in order to obtain short bunches with sufficiently low momentum spread.

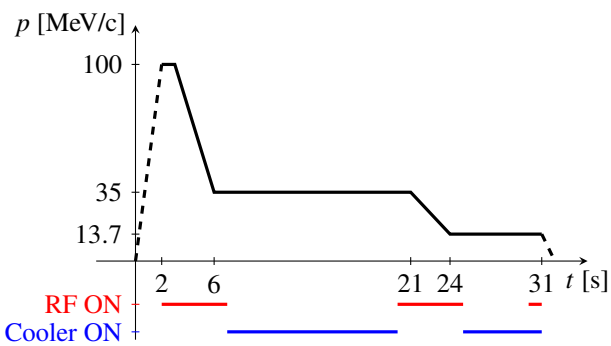

Figure 5: Typical ELENA pbar cycle. A solid black line indicates the period with circulating beam. RF and electron cooler are ON during the periods highlighted in red and blue, respectively. The time scale is an approximation of what was being used by the end of 2018.

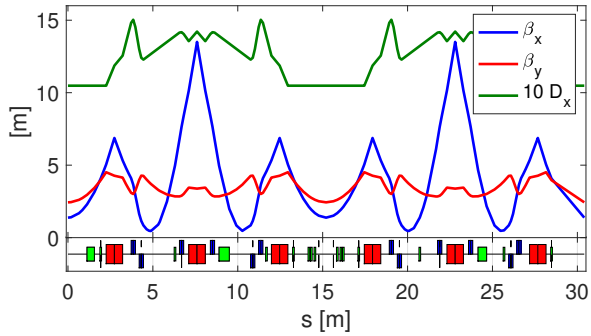

Figure 6: Design optics of ELENA Ring, starting from the middle of the injection section. The bottom layout shows the position of bending dipoles (red), orbit correctors and kickers (green) and quadrupoles (blue).

OPTICS CONTROL

The nominal transverse optics is shown in Fig. 6. No optics change is foreseen during the whole decelerating cycle.

After several iterative adjustments it was possible to obtain a tune stability along the cycle of the order of $\Delta Q < .02$ with respect to the desired tunes. Figure 7 shows a typical tune measurement obtained during the second deceleration ramp. The tune signal disappears at $t \approx 24500$ ms when the beam is debunched and the electron cooler is started. Beam-time availability and software limitations in the control system did not allow for a finer control of the tunes.

Coupling was empirically corrected by acting on skew quadrupoles settings while minimising the measurable separation between tunes and minimising the cross-talk between planes during tune measurements.

Chromaticity was measured by imposing an energy deviation. The obtained values agree reasonably well with expectation. No serious attempt to minimise chromaticity with sextupoles was done. So far, the empirical experience is that sextupoles do not help in improving beam transmission along the cycle.

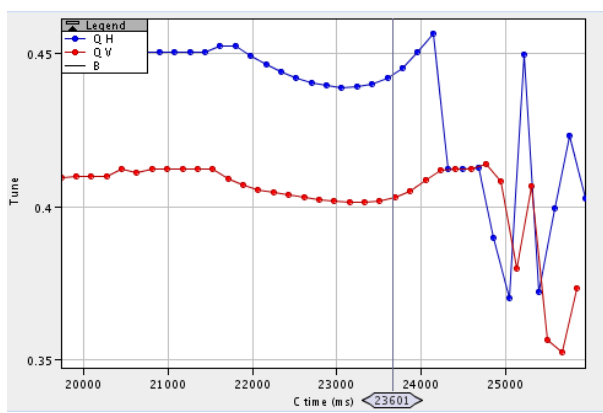

Figure 7: Measured tunes as a function of time during the second deceleration ramp with nominal optics.

ISBN: 978-3-95450-223-3 ISSN: 2673-7000 doi:10.18429/JACoW-NAPAC2019-WEYBB1

A few kick response matrix measurements were performed and are being currently analysed using Alhoa [24]. Preliminary results show qualitative agreement with the design optics. shown in Fig. 6.

One peculiarity of the sector bending magnets is the edge angles of 17 degrees [5]. This allows for having a closed optics even with quadrupoles not being powered ($\beta_{max} < 8$ m; $D_x \approx 2$ m; $Q_H = 1.84$, $Q_y = 1.73$). In this configuration it was possible to inject and decelerate more than 50% of the pbar beam down to the 35 MeV/c plateau. Measured tunes at injection were consistent with model predictions, while small deviations ($\Delta Q < .05$ shift) appeared at the arrival on the 35 MeV/c plateau, pointing to possible hysteresis effects in the bending magnets or stray fields from other sources.

ELECTRON COOLER SETUP

The ELENA electron cooler [25] was designed taking as inspiration the S-LSR electron cooler [26]. Special care was taken during the design of the electron gun [27] and the magnetic system in order to optimise the electron cooler performance, especially for the lowest beam energy of 100 keV. Magnetic measurements and corrections were performed prior of the installation in the ring in order to approach the tight design specification ($B_\perp/B_\parallel \leq 5e-4$) [28].

The careful work before installation allowed for a fast set-up of the electron beam in the e-cooler, after the necessary conditioning of the cathode. The perturbation to the circulating beam after powering the electron cooler magnetic system was corrected by setting the theoretical values of compensating solenoids and orbit correctors, plus some small empirical adjustment.

The electron beam velocity was adjusted to match the circulating beam velocity by looking at longitudinal Schottky signal. Alignment and overlap of the two beams were empirically adjusted with orbit bumps on the circulating beam while minimising the final emittance measured with the scraper. After all adjustments, the effect of cooling was clearly visible in both the transverse (e. g. Fig. 8) and longitudinal (e. g. Fig. 9) planes. The measured longitudinal cooling time of the order of a second is compatible with expectations. The limited beam-time did not allow for careful characterisation of the transverse cooling times. Dedicated

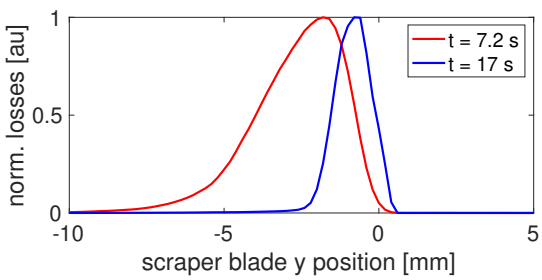

Figure 8: Normalised beam losses as a function of the vertical scraper position before (red) and after (blue) cooling. The width of the signal corresponds to half the beam size.

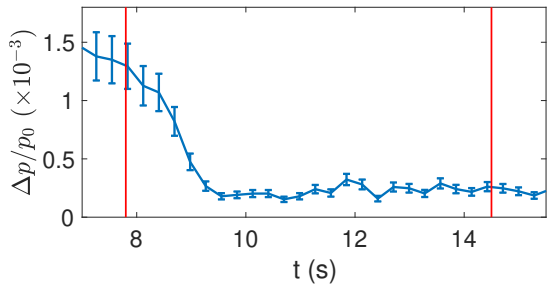

Figure 9: RMS momentum spread obtained from the longitudinal Schottky signal during the intermediate plateau with e-cooling. The start times of the scraper measurements in Fig. 8 are indicated in red.

analysis of the available data at the two cooling plateaus is documented in [18].

RF OPTIMISATION

The flexible LLRF system provides the capability to adjust and optimise several parameters. A precise B-Train system [5,29] yields the online dipole field which is used to compute the expected beam revolution frequency.

RF feedback loops were required to control the RF Cavity Voltage, the beam phase and beam energy during the different stages of the cycle. A careful adjustment of the loop gains over several iterations was needed to ensure beam stability and reproducibility [15]. In particular, the optimisation of the re-bunching after cooling was critical, also due to a B-Train drift during the plateau.

Several RF harmonics and longitudinal manipulation were tested, e. g. Fig. 10 shows an attempt of bunch rotation. Some mismatch and voltage distortions were observed for high RF voltages, which could be the source of the undesired

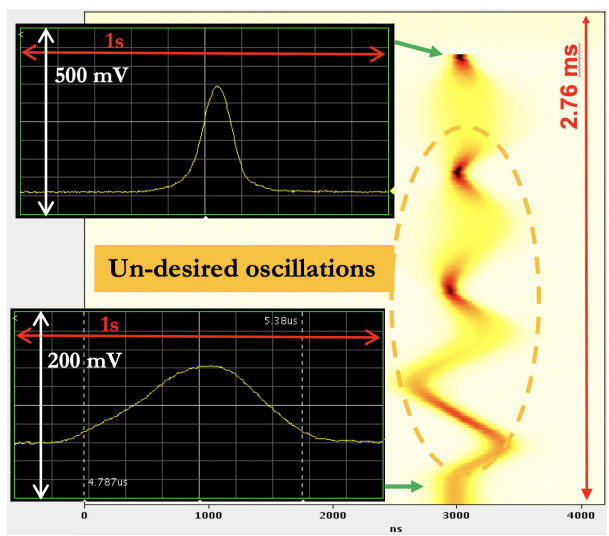

Figure 10: Tomoscope acquisition during an attempt of bunch rotation before extraction. The longitudinal profiles before rotation and before extraction are also shown.

ISBN: 978-3-95450-223-3 ISSN: 2673-7000 doi:10.18429/JACoW-NAPAC2019-WEYBB1

Table 1: Design [5] and Obtained [30] Beam Parameters Before LS2 for the pbar Cycle

Parameter	Design	Obtained
Q_x/Q_y	≈ 2.3/≈ 1.3	2.46/1.41
Cycle duration [s]	20	30
Injected intensity [pbars]	3e7	3.7e7
Efficiency [%]	60	50
Extracted bunches [#]	4	4
Bunch population [pbars]	0.45e7	0.43e7
$\Delta p/p_0$	5e-4	7e-4
Bunch length [ns]	75	85
ϵ_{phys} x/y [μm]	1.2/0.75	4.1/1.5

oscillations seen in Fig. 10 after the application of a voltage step. So far there is no indication that such distortions are a cause of beam losses or degradation.

Longitudinal emittance heating due to RF noise was a concern during conceptual design, but so far there are no strong indications of such an effect, except a probably slightly lower H^- lifetime than expected.

OBTAINED BEAM PERFORMANCES

Despite the little beam time availability and the issues with the ion source, and thanks to several empirical optimisations, by the end of 2018 it was possible to achieve beam parameters for the bunches before extraction which are reasonably close to the design values, see Table 1. Note that most measured values have a rather high uncertainty as very little statistics could be accumulated and not all diagnostics could be fully calibrated.

Figure 11 shows the typical beam transmission obtained along the deceleration cycle toward the end of the 2018 run. Note that the blue trace is affected by the bunch intensity but also by bunch length and number of bunches. The small signal during the second ramp is due to the use of the fourth RF harmonic ($h = 4$) instead of $h = 1$ as for the first ramp.

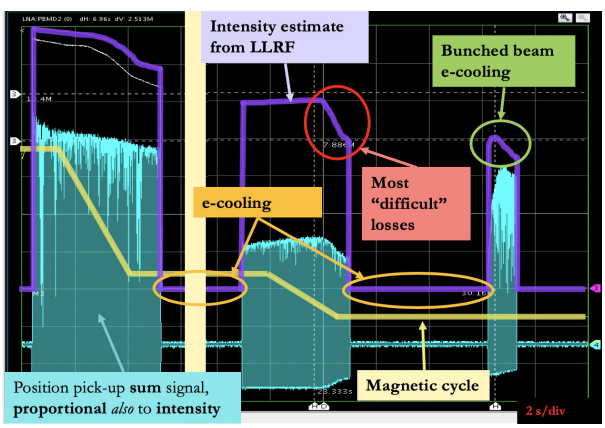

Figure 11: Beam intensity (purple) and magnetic cycle (yellow) as a function of time. The blue trace is the peak line density of the beam seen by one BPM.

Also during the final bunched beam cooling the RF was set to $h = 4$ and one can see the increase of the line density corresponding to the shortening of the bunches due to cooling. The use of $h = 4$ during the second ramp seemed to have a beneficial impact on transmission, even though considerable losses are still present toward the end of the ramp. Those losses were the most difficult to reduce for reasons which are still unclear.

CONCLUSIONS AND OUTLOOK

2018 was a very fruitful year for ELENA commissioning. Many sub-systems (RF, beam instrumentation, e-cooler) were commissioned and the parameters of the extracted beam were close to the design values, despite the limited available beam time. Transverse emittance reduction up to about 80 % was achieved even at the lowest plateau at 100 keV [18]. The final machine settings were obtained after several steps of systematic and empirical tuning of the available machine knobs, which surely left room for improvements.

During LS2 the main activity will be the installation of all electrostatic transfer lines toward the "old" AD experimental zone. Figure 12 shows a layout of the experimental areas next to the ELENA ring with all transfer lines being installed. The end of the installation with cabling is expected by mid 2020. This will allow to commission the transfer line with H^- beam before the restart of the AD, which is foreseen for April 2021. The transfer line commissioning with H^- will also allow for verifying if additional shielding due to magnetic stray field in the experimental area is necessary, and eventually act consequently [31]. Investigations are ongoing to hopefully solve the reliability and stability issue of the ion source, as well as to complete the development and production of the microwire monitor acquisition system.

ACKNOWLEDGEMENTS

The achievements of the ELENA commissioning were made possible only thanks to the dedication and effort of many groups and people. Particular mention to the CERN Electrical Power Converters (EPC) Group for their prompt assistance with the ion source insulation transformer.

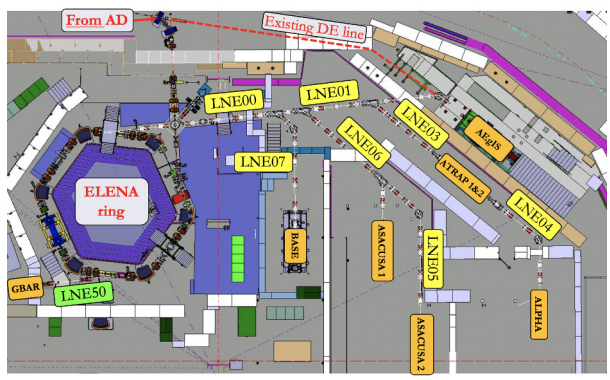

Figure 12: Layout of ELENA extraction lines. The lines being built during LS2 are highlighted in yellow.

ISBN: 978-3-95450-223-3 ISSN: 2673-7000 doi:10.18429/JACoW-NAPAC2019-WEYBB1

REFERENCES

[1] M. Hori and J. Walz, "Physics at CERN's Antiproton Decelerator", *Prog. Part. Nucl. Phys.*, vol. 72, pp. 206 - 253, Sep. 2013.

[2] B. Autin *et al.*, "The Antiproton Decelerator (AD), a Simplified Antiproton Source (Feasibility Study)", CERN, Geneva, Switzerland, Rep. CERN-PS-95-36-AR, Nov. 1995.

[3] Y. Bylinsky *et al.*, "RFQD: A 'Decelerating' radio frequency quadrupole for the CERN anti-proton facility", in *Proc. LINAC2000*, Monterey, USA, Aug. 2000, paper TUD05.

[4] M. Hori *et al.*, "Direct Measurement of Transition Frequencies in Isolated $\overline{p}\mathrm{He}^+$ Atoms, and New *CPT*-Violation Limits on the Antiproton Charge and Mass", *Phys. Rev. Lett.*, vol. 91, no. 12, p. 123401, Sep. 2003.

[5] V. Chohan (ed.) *et al.*, "Extra Low ENergy Antiproton (ELENA) ring and its Transfer Lines: Design Report", CERN, Geneva, Switzerland, Rep. CERN-2014-002, Jan. 2014.

[6] C. Carli *et al.*, "ELENA: Installations and Preparations for Commissioning", in *Proc. IPAC'16*, Busan, Korea, May 2016, paper MOPOY009, pp. 860–863.

[7] T. Eriksson *et al.*, "ELENA - From Installation to Commissioning", in *Proc. IPAC'17*, Copenhagen, Denmark, May. 2017, paper WEPVA034.

[8] D. Barna *et al.*, "Design and Optimization of Electrostatic Deflectors for ELENA", in *Proc. IPAC'15*, Richmond, VA, USA, May 2015, paper MOPJE043.

[9] M. Fraser *et al.*, "Beam Dynamics Studies of the ELENA Electrostatic Transfer Lines", in *Proc. IPAC'15*, Richmond, VA, USA, May 2015, paper MOPJE044.

[10] G. Tranquille *et al.*, "Commissioning the ELENA Beam Diagnostics Systems at CERN", in *Proc. IPAC'18*, Vancouver, Canada, Apr. 2018, paper WEPAF084.

[11] L. Søby *et al.*, "Elena Orbit and Schottky Measurement Systems", in *Proc. IPAC'15*, Richmond, VA, USA, May 2015, paper MOPTY056.

[12] O. Marqversen (ed.) *et al.*, "The Orbit Measurement System for the CERN Extra Low Energy Antiproton Ring". in *Proc. IBIC'17*, Grand Rapids, Michigan, USA, Aug. 2017, paper TUPCF05.

[13] R. Marco-Hernández *et al.*, "The AD and ELENA Orbit, Trajectory and Intensity Measurement Systems", J. Instrum., vol. 12, no. 07, p. P07024, Jul. 2017.

[14] S. Deghaye *et al.*, "Oasis: A New System to Acquire and Display the Analog Signals for LHCs". in *Proc. ICALEPCS'03*, Gyeongju, Korea, Oct. 2003, pp.359.

[15] M.E. Angoletta *et al.*, "The New Digital Low-Level RF System for CERN's Extra Low Energy Antiproton Machine," in *Proc. IPAC'19*, Melbourne, Australia, May 2019, paper THPRB069.

[16] J. Sanchez-Quesada, "ELENA Ring Longitudinal Pick-ups Commissioning Report", CERN, Geneva, Switzerland, EDMS 1740107, Jan. 2017.

[17] J.R. Hunt *et al.*, "Emittance Measurements in Low Energy Ion Storage Rings," *Nucl. Instr. Meth.*, vol. 896, pp. 139-151, Jul. 2018.

[18] J.R. Hunt *et al.*, "Emittance Evolution of Low Energy Antiproton Beams in the Presence of Deceleration and Cooling", in *Proc. IPAC'19*, Melbourne, Australia, May 2019, paper WEPGW090.

[19] M. Gasior and R. Jones, "High Sensitivity Tune Measurement by Direct Diode Detection", in *Proc. DIPAC'05*, Lyon, France, June, 2005, pp. 310-312.

[20] M. Hori, "Photocathode Microwire Monitor for Nondestructive and Highly Sensitive Spatial Profile Measurements of Ultraviolet, X-Ray, and Charged Particle Beams", *Rev. Sci. Instrum.*, vol. 76, no. 11, p. 113303, Nov. 2005.

[21] A. Megía-Macías, R. Gebel and B. Lefort, "The ion source for the commissioning of ELENA ring", in *Proc. ICIS'2017*, Geneva , Switzerland, Oct. 2017, vol. 2011, no.1, p. 090014.

[22] M.E. Angoletta *et al.*, "Initial Beam Results of CERN ELENA's Digital Low-Level RF System", in *Proc. IPAC'17*, Copenhagen, Denmark, May 2017, paper THPAB142.

[23] B. Latacz, "Status of the GBAR experiment at CERN", in *Proc. Moriond Gravitation 2019*, La Thuile, Italy, March 2019, eprint 1905.06404.

[24] K. Fuchsberger, "Aloha - Optics studies by combined kick-response and dispersion fits," CERN, Geneva, Switzerland, Rep. CERN-BE-Note-2009-020, Mar. 2009.

[25] G. Tranquille *et al.*, "The ELENA Electron Cooler", in *Proc. IPAC'16*, Busan, Korea, May 2016, paper TUPMR006.

[26] H. Fadil *et al.*, "Design of a compact electron cooler for the S-LSR", *Nucl. Instr. Meth.*, vol. 532, no. 1, pp. 446 - 450, June 2004.

[27] G. Tranquille *et al.*, "Design and Optimisation of the ELENA Electron Cooler Gun and Collector," in *Proc. IPAC'16*, Busan, Korea, May 2016, paper THPMB048.

[28] G. Tranquille *et al.*, "The CERN-ELENA Electron Cooler Magnetic System", in *Proc. IPAC'18*, Vancouver, Canada, Apr. 2018, paper TUPAF056.

[29] C. Grech *et al.*, "A Magnetic Measurement Model for Real-Time Control of Synchrotrons", IEEE TIM, to be published.

[30] *Extended ECC meeting*, 7 March 2019, `https://indico.cern.ch/event/803767/`.

[31] J. Jentzsch *et al.*, "Beam Dynamics Studies of the ELENA Electrostatic Transfer Lines in the Presence of Magnetic Stray Fields", in *Proc. IPAC'16*, Busan, Korea, May 2016, paper THPMB047.